

Primordial black holes and secondary gravitational waves from the inflation potential with a tiny bump

Wei Yang^{a*}, Yu-Xuan Kang^{b†}, Arshad Ali^{c‡}, Tao-Tao Sui^{a§}, Chen-Hao Wu^{a¶}, and Ya-Peng Hu^{a,d**}

^a*College of Physics, Nanjing University of Aeronautics and Astronautics, Nanjing, 211106, China*

^b*School of Physics Sciences, University of Science and Technology of China, Hefei 230026, China*

^c*Institute for Advanced Study & School of Physical Science and Technology,*

Soochow University, Suzhou 215006, P.R. China

^d*Key Laboratory of Aerospace Information Materials and Physics (NUAA), MIIT, Nanjing 211106, China*

This paper explores the generation of primordial black holes (PBHs) and scalar-induced gravitational waves (SIGWs) from the inflation potential with a tiny bump. We propose a Lorentz function that makes a tiny bump characteristic of the inflation model potential. This property makes the scalar field move locally ultra slowly, which not only makes the primordial curvature power spectrum have $\mathcal{O}(10^{-2})$ peaks at a small scale but also satisfies observational constraints of the cosmic microwave background (CMB) on a large scale. Specifically, we calculate the abundances of PBHs for different mass ranges in this model, where PBHs with mass $10^{-12}M_{\odot}$ can make up almost all dark matter and PBHs with mass $10^{-5}M_{\odot}$ can explain OGLE ultrashort-timescale microlensing events. Moreover, we find that SIGWs accompanying the PBHs can be tested by the Square Kilometre Array (SKA), TianQin, Taiji, Laser Interferometer Space Antenna (LISA), and DECIGO. As for the parameter set I, the consequent SIGWs can explain the NANOGrav 12.5yrs signal.

PACS numbers:

I. INTRODUCTION

The investigation of gravitational waves (GWs) has played a pivotal role in cosmology and astrophysics since the formulation of the theory of general relativity in the 20th century. The Laser Interferometer Gravitational-Wave Observatory (LIGO) achieved a historic milestone by successfully detecting GW signals originating from binary black hole mergers [1]. Subsequently, the LIGO/Virgo collaborations extended this achievement to encompass mergers involving black holes and neutron stars, ushering in a new era of multi-messenger astronomy [2]. Notably, the emergence of GW signals from such events has spurred heightened interest in primordial black holes (PBHs) as they are posited to explain binary black hole mergers [3, 4].

Several astrophysical observations provide credible evidence that dark matter (DM) is the non-negligible element of our universe [5–7]. As viable candidates of cold DM, PBHs have also attracted lots of attention [8–15]. A large number of different types of cosmological and astronomical observations have been made on the abundance of primordial black holes as dark matter in many mass ranges. Limit is given [16–23]. However, the abundances of PBHs at the mass windows of $10^{-17} - 10^{-15}M_{\odot}$ and $10^{-14} - 10^{-12}M_{\odot}$ are largely unconstrained by observations and specific assumptions, and can be explained almost all elements

of the DM [24], and PBHs with planetary masses can explain the ultrashort-timescale microlensing events in the OGLE data [25].

There are many PBH formation mechanisms, the most popular one is the overdense region gravitational collapse inside a Hubble horizon, where the density exceeds the threshold value [26]. Many situations can form the overdense region, such as enhancement of curvature perturbation [27–29], accumulation of topological defect [30–33], and postponed false vacuum decay during first-order transition [34, 35]. Beyond PBHs, these perturbations also contribute to the production of scalar-induced gravitational waves (SIGWs) [36–41], which can be tested by space-based GW detectors, such as the Laser Interferometer Space Antenna (LISA) [42], Taiji [43], TianQin [44], and Deci-hertz Interferometer Gravitational-Wave Observatory (DECIGO) [45] in the future. To produce a sufficient abundance of PBHs as DM and detectable SIGWs, we need a sufficient large-density perturbation at a small scale.

The traditional single-field and multi-field inflation models can enhance curvature perturbations by fine-tuning the parameters [46–50]. The form of perturbation of the potential function is not unique [51, 52]. Some people use Gaussian and Lorentz functions to construct antisymmetric perturbations [48, 53]. In this paper, we propose a tiny bump in the form of a Lorentz function as a local correction of the basic inflation potential $V_b(\phi)$, which can create a perfect platform in the inflation potential function to bring inflation into the ultra-slow roll (USR) phase, and it exhibits good symmetry in the USR region for ϕ_0 . Nevertheless, we find that this property does not affect the inflation potential to satisfy the cosmic microwave background (CMB) observation constraints on a large scale, but also leads to peaks in the curvature

*yw1214@nuaa.edu.cn

†yxkang@mail.ustc.edu.cn

‡arshadali@suda.edu.cn

§taotaosui@nuaa.edu.cn

¶chenhao.wu@nuaa.edu.cn

**huyp@nuaa.edu.cn, corresponding author

power spectrum. We use three sets of parameters to numerically calculate the corresponding peaks of the power spectrum of the primordial curvature perturbations, and find that they all reach $\mathcal{O}(10^{-2})$ on a small scale. It is worth noting that the enhancement of the curvature perturbations corresponding to different scales also promotes the generation of PBHs with different masses and SIGWs with different frequencies.

This paper is organized as follows. In section II, we propose a bump function and calculate the slow-roll parameters. In section III, we numerically calculate the power spectrum of the primordial curvature perturbations, n_s , r and the abundance of PBH. In section IV, we study the energy density spectrum of SIGWs. Finally, we draw our conclusion and discussion in section V.

II. A TINY BUMP IN POTENTIAL AND SLOW ROLL INFLATION

In this paper, we study single-field inflation, and its corresponding action is

$$S = \int d^4x \sqrt{-g} \left[\frac{1}{2}R - \frac{1}{2}g_{\mu\nu} \nabla^\mu \phi \nabla^\nu \phi - V(\phi) \right]. \quad (1)$$

Our model of a small local perturbation forming PBH is based on potential with the general form [51]

$$V(\phi) = V_b(1 + f(\phi)). \quad (2)$$

We have considered this general form of the potential as a phenomenological model. Where V_b is the base inflation potential responsible for generating quantum fluctuations compatible with the CMB constraints, Here $f(\phi)$ represents a tiny local bump, so here it's a small quantity much smaller than 1.

Of the numerous inflation models, the Starobinsky inflation model is almost the most well-known one and it is well-aligned with current CMB measurements [54, 55]. Thus, we choose the base potential V_b in Eq.(2) is associated with this inflation model

$$V_b = \frac{3}{4}m^2 \left(1 - e^{-\sqrt{\frac{2}{3}}\phi} \right)^2, \quad (3)$$

where $m = 1.13 \times 10^{-5}m_p$, denotes the mass parameter. Here, we adopt the reduced Planck mass as $m_p = \frac{1}{\sqrt{8\pi G}} = 1$. We suggest a new function form of this local bump as

$$f(\phi) = bL(\sqrt{c}(\phi - \phi_0)) = \frac{b}{1 + c(\phi - \phi_0)^2}, \quad (4)$$

where $L(\sqrt{c}(\phi - \phi_0))$ is a Lorentz function, which Lorentz function acts as a local bump in the potential function, and to ensure that the potential function can enter a relatively flat platform, the value of c should be much larger than 1 to ensure that the width of the peak is relatively large. ϕ_0 controls the bump position of the potential function, which is also a field value in inflation,

and b represents the amplitude, and the nature of the small perturbations causes b to be limited to a range of $0 < b \ll 1$. Notably, when $b = 0$, the model reduces to the Starobinsky inflation model for the Eq.(2). This feature of the local bump will cause the inflation potential to enter the USR phase near the ϕ_0 , and we will introduce slow rolling inflation below.

In the context of a spatially flat homogeneous and isotropic universe with FLRW metric $ds^2 = -dt^2 + a(t)\delta_{ij}dx^i dx^j$, the Friedmann equation and dynamical equations of the inflation field ϕ are as follows [27]

$$\begin{aligned} 3H^2 &= \frac{1}{2}\dot{\phi}^2 + V(\phi), \\ \dot{H} &= -\frac{1}{2}\dot{\phi}^2, \\ \ddot{\phi} + 3H\dot{\phi} + V_\phi(\phi) &= 0. \end{aligned} \quad (5)$$

Here, $a(t)$ is the scale factor, and $H = \dot{a}/a$ represents the Hubble parameter. For the homogeneous background, the inflation field is only time-dependent, $\phi = \phi(t)$. During the inflation epoch, the scalar field's movement is characterized by extreme slowness, with the potential energy being the dominant contributor to the scalar field's energy. The scalar field adheres to the slow-roll condition, which entails $\frac{1}{2}\dot{\phi}^2 \ll V(\phi)$ and $|\ddot{\phi}| \ll 3H|\dot{\phi}|$. The dynamics equations to approximate [28, 50]

$$3H^2 \simeq V(\phi), \quad 3H\dot{\phi} \simeq -V_\phi(\phi). \quad (6)$$

The slow-roll parameters are defined as

$$\epsilon_H = -\frac{\dot{H}}{H^2}, \quad \eta_H = -\frac{\ddot{\phi}}{H\dot{\phi}}. \quad (7)$$

The $\epsilon_H \ll 1, |\eta_H| \ll 1$ during inflation, the end of inflation condition is $\epsilon_H = 1$. In this paper, we choose the initial value time of inflation $\phi_* = 5.42$, which makes $\epsilon_H(\phi_*) \approx 10^{-4}$ satisfies the slow-roll condition, and we can obtain $\phi_{\text{end}} = 0.614$ by $\epsilon_H(\phi_{\text{end}}) = 1$. Therefore, the parameter ϕ_0 of the bump function has a range value of $0.614 < \phi_0 < 5.42$. According to the above constraints of b and c , we choose an optimal set of parameters, $b = 4 \times 10^{-4}$, $c = 10013.8$, $\phi_0 = 5.1$, and they are brought into Eq.(4) to satisfy $f(\phi) \ll 1$. The evolution of the potential function containing a bump for ϕ as shown in Fig.1, It is not difficult to see that the potential function changes very little near ϕ_0 , which will also lead to The number of e-folds is superimposed during inflation, according to the formula of number of e-folds

$$N = \int_{\phi_*}^{\phi_{\text{in}}} \frac{1}{\sqrt{2\epsilon_H}} d\phi, \quad (8)$$

where ϕ_{in} is scalar field values in inflation. Fig.2(a) visually represents that the value change of the inflation field is very small and the number of e-folds increases around $\Delta N \approx 10$ e-folds near the $\phi_0 \approx 5.1$. However, it will not make the total number of e-folds by the end of inflation

too large, when the ϕ_{in} closer to ϕ_{end} can keep the total number of e-folds N around 60, that satisfy the CMB constraints. This implies that the slow-roll parameter ϵ_H will have a minimum value in the corresponding region, as shown in Fig.2(b). The ϵ_H satisfies the inflation condition $\epsilon_H \ll 1$ during inflation and $\epsilon_{Hmin} \sim 10^{-10}$, that provides favorable conditions for the calculation of the primordial curvature power spectrum.

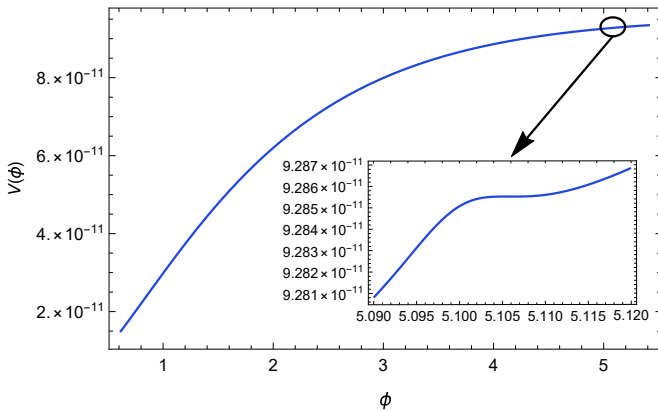


FIG. 1: The evolution of the potential function containing a bump for ϕ . The small figures show the behavior of the potential around the ϕ_0 , and the parameters are $b = 4 \times 10^{-4}$, $c = 10013.8$, $\phi_0 = 5.1$.

The well-known slow-roll approximation formula for the power spectrum of primordial scalar perturbation is given by [27, 28]

$$P_\zeta = \frac{H^2}{8\pi^2\epsilon_H}. \quad (9)$$

It is inversely proportional to the slow-roll parameter ϵ_H , and due to the flattening of the potential energy near ϕ_0 , the Hubble parameter H can be approximated as constant from Eq.(6). The $\epsilon_{Hmin} \sim 10^{-10}$ near ϕ_0 , signifying a reduction of six orders of magnitude compared to the initial value of $\epsilon_H(\phi_*)$. Thus, we obtain the approximated results of the power spectrum is $\mathcal{O}(10^{-3})$, which does not reach $\mathcal{O}(10^{-2})$. In addition, although when entering an ultra-slow roll period, the $\epsilon_H \ll 1$ implies inflation does not end. But the $|\eta_H|$ is greater than 1 for a short period which seems to violate the slow roll condition as shown in Fig.2(c). Therefore, Eq.(9) cannot be used to calculate the power spectrum [28, 50], we will calculate the power spectrum numerically in the next section.

III. THE POWER SPECTRUM AND PRIMORDIAL BLACK HOLES

In this section, we first investigate the behavior of the power spectrum for primordial curvature perturbation to ensure it satisfies the constraints of CMB observations. By numerically solving the Mukhanov-Sasaki equation

[56, 57]

$$\frac{d^2 v_k}{d\eta^2} + \left(k^2 - \frac{1}{z} \frac{d^2 z}{d\eta^2} \right) v_k = 0, \quad (10)$$

where the conformal time $d\eta = dt/a$, the quantum canonical field $v_k = z\zeta_k$ and $z = a\dot{\phi}/H$, we can obtain the scalar power spectrum

$$P_\zeta = \frac{k^3}{2\pi^2} \frac{|v_k|^2}{z^2}. \quad (11)$$

In this work, we use three suitable sets of parameters I, II, and III in Table I, and numerically calculate the power spectrum. We find that three sets of parameters can not only eliminate the contingency of the single set of parameters model but also broaden the peak scale k_{peak} range corresponding to the peak of the power spectrum P_{peak} . In Fig.3, we show the power spectrum results of numerical calculation for models I, II, and III with blue, red, and black lines, respectively. We find the peak values of the power spectrum to reach the order of $\mathcal{O}(10^{-2})$ at the scales $k_{peak} \sim 10^5 \text{ Mpc}^{-1}$, $k_{peak} \sim 10^8 \text{ Mpc}^{-1}$ and $k_{peak} \sim 10^{12} \text{ Mpc}^{-1}$ as shown in Table I.

The local bump of the potential function causes the power spectrum to have a peak, and the effect on large-scale cosmic microwave background (CMB) is discussed below. Compared with Planck 2018 CMB observation constraints with a pivot scale of $k = 0.05 \text{ Mpc}^{-1}$, which provide constraints such as the scalar spectral index $n_s = 0.9649 \pm 0.0042$ (68% CL) and tensor-to-scalar ratio $r_{0.05} < 0.06$ (95% CL) at large scale [58, 59]. The relevant CMB parameters, n_s and r are [50]

$$\begin{aligned} n_s &= 1 + \frac{d \ln P_\zeta}{d \ln k} \simeq 1 + 2\eta_H - 4\epsilon_H, \\ r &= \frac{P_T}{P_\zeta} \simeq 16\epsilon_H. \end{aligned} \quad (12)$$

We numerically calculate the scalar spectral index n_s and the tensor-to-scalar ratio r as shown in Table I, which satisfy the constraints of Planck 2018 CMB observations. The significance and richness of the primordial curvature perturbation power spectrum peak results indicate that the dark matter abundance of primordial black holes should have corresponding significant results.

Next, we explore the abundance of PBHs within the context of the model. PBHs could form due to the amplification of small-scale curvature perturbations during the inflation process, and they can emerge if the density perturbations exceed a certain threshold. We have ignored non-Gaussian effects in our analysis for simplicity. As previously mentioned, the comoving curvature perturbation in our model is assumed to follow the Gaussian distribution. The most simple method to estimate β is to use the Press-Schechter formalism, the fractional energy density of PBHs of the universe is [28, 63]

$$\beta = \frac{\rho_{PBH}}{\rho_{tot}} \approx \text{erfc} \left(\frac{9\delta_c}{4\sqrt{2}P_\zeta} \right) \approx \sqrt{\frac{2}{\pi}} \frac{\sqrt{P_\zeta}}{\mu_c} e^{-\frac{\mu_c^2}{2P_\zeta}}, \quad (13)$$

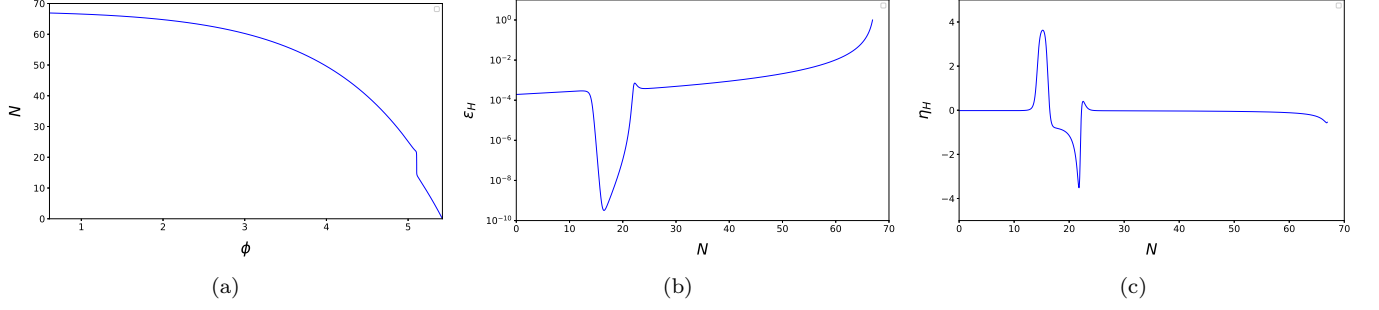


FIG. 2: (a) shows the evolutions of e-folds number N . (b) shows the evolutions of the first slow-roll parameter ϵ_H . (c) shows the evolutions of the second slow-roll parameter η_H .

TABLE I: Model parameters and the numerical results

set	$b(10^{-4})$	c	ϕ_0	N	n_s	r	$k_{\text{peak}}/\text{Mpc}^{-1}$	$P_{\zeta(\text{peak})}$	$\frac{M_{\text{peak}}}{M_{\odot}}$	$Y_{\text{PBH}}^{\text{peak}}$	f_c/Hz
I	4	10013.8	5.1	67	0.967906	0.003023	3.13×10^5	0.018	37.51	0.00059	4.84×10^{-10}
II	4.1	16824	4.89	62	0.967879	0.003024	5.57×10^8	0.015	1.186×10^{-5}	0.026	8.61×10^{-7}
III	4.4	34131.8	4.63	61	0.967876	0.003024	1.42×10^{12}	0.013	1.83×10^{-12}	0.862	2.19×10^{-3}

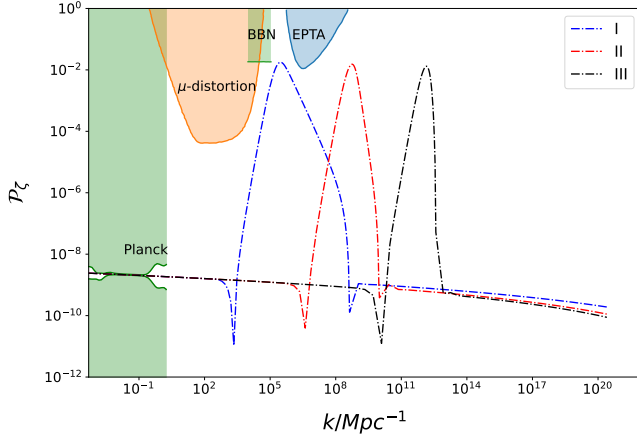


FIG. 3: The scalar power spectrum in the models, are enhanced to $\mathcal{O}(10^{-2})$ on small scales. The dashed line represents the power spectrum, and the shaded regions represent the observation constraint [58, 60–62].

where ρ_{tot} and ρ_{PBH} represent the energy density of the cosmic background and PBHs, respectively. The $\text{erfc}(x)$ is the complementary error function and $\mu_c = 9\delta_c/4$ in the radiation-dominated period [28]. The threshold of density perturbation for the formation of the PBHs can be $\delta_c = 0.4$ [64].

The PBHs abundance is given as [13, 28]

$$Y_{\text{PBH}} = \frac{\beta}{3.94 \times 10^{-9}} \left(\frac{\gamma}{0.2} \right)^{\frac{1}{2}} \left(\frac{g_*}{10.75} \right)^{-\frac{1}{4}} \times \left(\frac{0.12}{\Omega_{\text{DM}} h^2} \right) \left(\frac{M_{\text{PBH}}}{M_{\odot}} \right)^{-\frac{1}{2}}. \quad (14)$$

In this equation, the numerical factor $\gamma = 0.2$, the effective degrees of freedom $g_* = 107.5$ for $T > 300 \text{ GeV}$ and $g_* = 10.75$ for $0.5 \text{ MeV} < T < 300 \text{ GeV}$ [65], Planck measurements provide the following value for the dark matter abundance $\Omega_{\text{DM}} h^2 = 0.12$ [66], $h = H/100 = 0.6727 \text{ km} \cdot \text{s}^{-1} \cdot \text{Mpc}^{-1}$, which measures the Hubble rate in units of 100, and M_{PBH} and M_{\odot} are the mass of PBHs and solar mass, respectively.

The relationship between mass and scale of PBHs is given by

$$M_{\text{PBH}} = 3.68 \left(\frac{\gamma}{0.2} \right) \left(\frac{g_*}{10.75} \right)^{-\frac{1}{6}} \left(\frac{k}{10^6 \text{ Mpc}^{-1}} \right)^{-2} M_{\odot}. \quad (15)$$

Combine the numerical results of the power spectrum and Eq.(13) and Eq.(15), we can obtain the peak mass of PBHs, as shown in Fig.4 and Table I. We find that the three sets of parameters we choose make the peak scale k_{peak} cover more ground, and also have the wider mass range of the PBHs. In other words, PBHs with different masses correspond to different peak scales k_{peak} , which will give our results a wider scope of application to explain the PBHs theory. Specifically speaking, for set I, PBHs with the stellar mass of approximately $30 M_{\odot}$ can be generated. These PBHs might be explained to the LIGO events [3, 4]. For set II, our model produces PBHs with the mass $M_{\text{PBH}} \sim 10^{-5} M_{\odot}$, which can explain OGLE ultrashort-timescale microlensing events[25] and be interpreted as Planet 9 that a hypothetical outer solar system object used to explain the anomalous orbits of trans-Neptunian objects [67]. For set III, PBHs with masses around $10^{-13} - 10^{-11} M_{\odot}$ make up almost all Dark Matter, and the peak abundance is approximately

$Y_{\text{PBH}} \approx 1$.

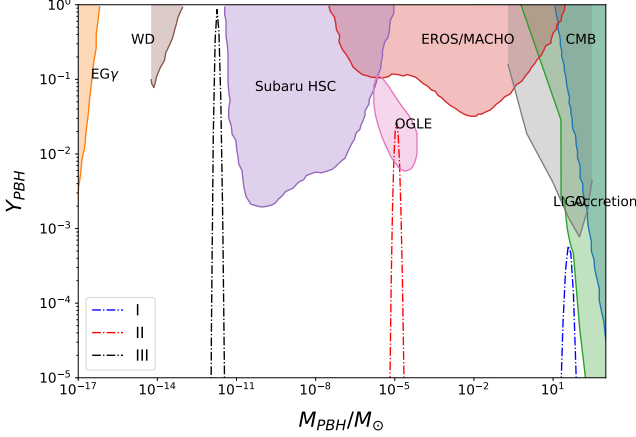


FIG. 4: The abundances of PBH produced by models. The dashed line represents the PBH abundance, and the shaded regions represent the constraints on PBHs from various observations[14, 16–23, 25]

IV. SCALAR-INDUCED GRAVITATIONAL WAVES

In this section, to investigate the energy density of SIGWs, we shed light on the production of SIGWs. The primordial scalar perturbation starts to evolve after re-entering the event horizon, and its transverse traceless component induces a stochastic gravitational wave background that can be observed by different detectors when the small-scale density perturbation is large enough. Here, we consider the perturbed metric in Newtonian gauge in the cosmological background which reads [68]

$$ds^2 = -a^2(\eta)(1 + 2\Phi)d\eta^2 + a^2(\eta) \left[(1 - 2\Phi)\delta_{ij} + \frac{1}{2}h_{ij} \right] dx^i dx^j, \quad (16)$$

where $a(\eta)$ is the scale factor of the universe. The scalar perturbation Φ is of the first order, and the transverse traceless part h_{ij} is the second-order tensor mode. In the following, in the evaluations of SIGWs, first, we briefly analyze the well-known results on h_{ij} . The Fourier component equation of h_{ij} can be expressed as

$$h_{ij}(\eta, \mathbf{x}) = \int \frac{d^3k}{(2\pi)^{3/2}} [e_{ij}^+(\mathbf{k})h_{\mathbf{k}}^+(\eta) + e_{ij}^\times(\mathbf{k})h_{\mathbf{k}}^\times(\eta)] e^{i\mathbf{k}\cdot\mathbf{x}}, \quad (17)$$

where the polarization tensors are defined as [50, 68]

$$e_{ij}^+(\mathbf{k}) = \frac{1}{\sqrt{2}}[e_i(\mathbf{k})e_j(\mathbf{k}) - \bar{e}_i(\mathbf{k})\bar{e}_j(\mathbf{k})], \quad (18)$$

$$e_{ij}^\times(\mathbf{k}) = \frac{1}{\sqrt{2}}[e_i(\mathbf{k})\bar{e}_j(\mathbf{k}) + \bar{e}_i(\mathbf{k})e_j(\mathbf{k})], \quad (19)$$

with $e_i(\mathbf{k})$ and $\bar{e}_i(\mathbf{k})$ being normalized vectors orthogonal to each other and to k . Satisfying $e_i(\mathbf{k}) \cdot \bar{e}_i(\mathbf{k}) = e_i(\mathbf{k}) \cdot \mathbf{k} = \bar{e}_i(\mathbf{k}) \cdot \mathbf{k}$. From perturbation of the Einstein's field equations $G_{\mu\nu} = 8\pi G T_{\mu\nu}$ to the second order, the Fourier component equation of the second order tensor perturbation h_k is [68–70]

$$h_{\mathbf{k}}''(\eta) + 2\mathcal{H}h_{\mathbf{k}}'(\eta) + k^2h_{\mathbf{k}}(\eta) = 4S_{\mathbf{k}}(\eta), \quad (20)$$

where, ' denotes $\frac{d}{d\eta}$, η is conformal time $\eta = \int dt/a(t)$, and the conformal Hubble parameter is $\mathcal{H} = a'/a$, and the source term is [68]

$$S_{\mathbf{k}} = \int \frac{d^3q}{(2\pi)^{3/2}} e_{ij}(\mathbf{k})q_iq_j \left[2\Phi_{\mathbf{q}}\Phi_{\mathbf{k}-\mathbf{q}} + (\mathcal{H}^{-1}\Phi'_{\mathbf{q}} + \Phi_{\mathbf{q}})(\mathcal{H}^{-1}\Phi'_{\mathbf{k}-\mathbf{q}} + \Phi_{\mathbf{k}-\mathbf{q}}) \right]. \quad (21)$$

During the radiation-dominated era, the scalar perturbation satisfies the following equation of motion in Fourier space to be expressed as

$$\Phi_k'' + 4\mathcal{H}\Phi_k' - \frac{k^3}{3}\Phi_k = 0, \quad (22)$$

where $\Phi_{\mathbf{k}}$ is the Fourier component of the gravitational potential, and it can be related to its primordial value ϕ_k by the transfer function

$$\Phi_{\mathbf{k}} = \Phi(k\eta)\phi_{\mathbf{k}}. \quad (23)$$

The transfer function for the radiation-dominated period is given by

$$\Phi(k\eta) = \frac{9}{(k\eta)^2} \left(\frac{\sin(k\eta/\sqrt{3})}{k\eta/\sqrt{3}} - \cos(k\eta/\sqrt{3}) \right), \quad (24)$$

and its two-point correlation function is determined by the power spectrum of the curvature perturbation

$$\langle \phi_{\mathbf{k}}\phi_{\mathbf{k}'} \rangle = \delta(\mathbf{k} + \mathbf{k}') \frac{2\pi^2}{k^3} \left(\frac{3 + 3w}{5 + 3w} \right)^2 P_\zeta(k). \quad (25)$$

The power spectrum of induced gravitational waves can be written as

$$\langle h_{\mathbf{k}}^\lambda(\eta)h_{\mathbf{k}'}^{\lambda'}(\eta) \rangle = \delta_{\lambda\lambda'}\delta^{(3)}(\mathbf{k} + \mathbf{k}') \frac{2\pi^2}{k^3} P_h(k, \eta), \quad (26)$$

where $\lambda, \lambda' = +, \times$ represents the polarization index, which we omit in the following. We solve the tensor Eq.(20) by employing the Green's function method, we obtain $h_{\mathbf{k}}(\eta)$ is expressed as

$$h_{\mathbf{k}}(\eta) = \frac{4}{a(\eta)} \int_{\eta}^{\eta} d\bar{\eta} G_k(\eta, \bar{\eta}) a(\bar{\eta}) S_{\mathbf{k}}(\bar{\eta}), \quad (27)$$

during the radiation-dominated period, the Green's function of GW is

$$G_k(\eta, \bar{\eta}) = \frac{\sin[k(\eta - \bar{\eta})]}{k}. \quad (28)$$

The fraction of the GW energy density is [68, 71]

$$\Omega_{\text{GW}}(k, \eta) = \frac{1}{24} \left(\frac{k}{a(\eta)H(\eta)} \right)^2 \overline{P_h(k, \eta)}. \quad (29)$$

Substituting the solution Eq.(27) into Eq.(26), Then the calculated the power spectrum for the SIGWs P_h is brought into Eq.(29) to obtain the fraction of energy density [68, 72]

$$\begin{aligned} \Omega_{\text{GW}}(k) = & \frac{1}{6} \left(\frac{k}{aH} \right)^2 \int_0^\infty dv \int_{|1-v|}^{1+v} du \\ & \left\{ \left[\frac{4v^2 - (1 - u^2 + v^2)^2}{4uv} \right]^2 \right. \\ & \left. \times I_R^2(u, v, x \rightarrow \infty) \mathcal{P}_\zeta(kv) \mathcal{P}_\zeta(ku) \right\}, \end{aligned} \quad (30)$$

where $u = |\mathbf{k} - \tilde{\mathbf{k}}|$, $v = \tilde{k}/k$, $x = k\eta$, and I_R is kernel function. The current frequency f and wave number k of the induced gravitational wave satisfy the following equation [73]

$$f = 1.546 \times 10^{-15} \frac{k}{1 \text{ Mpc}^{-1}} \text{ Hz}. \quad (31)$$

The fractional energy density of SIGWs today

$$\Omega_{\text{GW},0}(k) = \frac{\Omega_{\text{r},0}(k)}{\Omega_{\text{r}}(k)} \Omega_{\text{GW}}(k) \quad (32)$$

where $\Omega_{\text{r},0}(k) = 9.17 \times 10^{-5}$ is the current fractional energy density of radiation, and we choose $\Omega_{\text{r}}(k) = 1$ during the radiation domination[50, 74]. By substituting the numerical results of the power spectrum into Eq.(32), we obtain the energy density $\Omega_{\text{GW},0}$ of the SIGWs for the corresponding model and the peak frequencies f_c of these SIGWs are shown in Table I, we see that the peak frequencies of the SIGWs are nHz, μHz and mHz, respectively.

In this part, we show the predictions of the energy density spectrum of GWs for the above-mentioned parameters in Fig.5 and compare them with the constraints and future sensitivity curves for the GW observatories. As for the parameter set I, the consequent SIGWs (blue) can explain the NANOGrav 12.5yrs signal and can be tested by SKA. The model with parameter set III can be tested by LISA/Taiji/TianQin/ DECIGO.

V. CONCLUSION AND DISCUSSION

In this paper, we focus on the generation of PBHs and SIGWs within an inflation potential bump. We propose a simple Lorentz function form of bump as a local correction of the base inflation potential, which can show good symmetry about ϕ_0 in the USR region. At the same time, Our numerical results for the scalar spectral

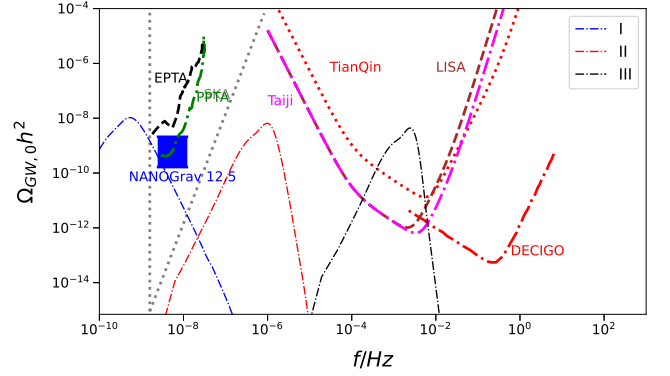


FIG. 5: The energy density spectrum of SIGWs. The curves show the sensitivity of current and future GW observatories. The black dashed curve, the green dot-dashed curve, and gray dotted curve denotes the EPTA limit [75–79], PPTA [80] and the SKA limit[81], respectively. The other limits from the TianQin [44], Taiji [43], the DECIGO[45], the LISA [42] and the aLIGO [1, 2], respectively. The blue region is the observational result from the North American Nanohertz Observatory for Gravitational Wave (NANOGrav) 12.5-year data[82]

index n_s and tensor-to-scalar ratio r predicted by this model align with the Planck 2018 results. Furthermore, our inflation mechanism enhances the power spectrum of the primordial curvature perturbation to $\mathcal{O}(10^{-2})$ at the scales $k_{\text{peak}} \sim 10^5 \text{ Mpc}^{-1}$, $k_{\text{peak}} \sim 10^8 \text{ Mpc}^{-1}$ and $k_{\text{peak}} \sim 10^{12} \text{ Mpc}^{-1}$, that satisfies the prerequisites for generating PBHs.

Subsequently, we derive that the abundances of PBH with stellar mass, planetary mass, and $10^{-12} M_\odot$ are $\mathcal{O}(10^{-4})$, $\mathcal{O}(10^{-2})$, and approximately 1, respectively. The PBHs with mass $10^{-12} M_\odot$ can make up almost all dark matter, and PBHs with mass $10^{-5} M_\odot$ can explain OGLE ultrashort-timescale microlensing events and can be explained to Planet 9. As is widely recognized, PBHs originate from matter collapse triggered by high-density perturbations in the early universe. It is important to note that the process of PBH formation is concomitant with the generation of SIGWs. Leveraging the PBHs mass distribution and the primordial curvature power spectrum, we have extracted the characteristics of the gravitational wave signal, focusing on the frequency and amplitude. Promisingly, we get these SIGWs that can be tested by gravitational wave observatories like SKA, Tianqin, Taiji, LISA, and DECIGO. As for the parameter set I, the consequent SIGWs (blue) can explain the NANOGrav 12.5yrs signal.

We give a new function form of the local correction term of the inflation model, this function does not depend on the concrete form of the model, and we can try to apply it in more models. In addition, we have ignored non-Gaussianity and quantum stochastic effects in our analysis for simplicity, which is to be examined in the future. Future studies could include these effects to obtain

more precise results for PBH formation with our bump potential[83–86]. The different calculation methods of PBH mass fraction β often lead to different final results. We have used the Press-Schechter (PS) theory to calculate in our present study. Hence, it will be challenging and meaningful work to use other theories such as peak theory [87, 88] to calculate β in this model and compare it with the results of the PS theory. These questions deserve further investigation in future research.

Acknowledgements

We would like to thank Dr. Zhu Yi and our group members for their assistance. This work is supported

by the National Natural Science Foundation of China (NSFC) under Grant No. 12175105, No. 11575083, No. 11565017, No. 12147175, Ya-Peng Hu is supported by the Top-notch Academic Programs Project of Jiangsu Higher Education Institutions (TAPP).

-
- [1] B. P. Abbott et al. (LIGO Scientific, Virgo), Observation of Gravitational Waves from a Binary Black Hole Merger, *Phys. Rev. Lett.* **116**, 061102 (2016), [arXiv:1602.03837 \[gr-qc\]](#).
 - [2] B. P. Abbott et al. (LIGO Scientific, Virgo), GWTC-1: A Gravitational-Wave Transient Catalog of Compact Binary Mergers Observed by LIGO and Virgo during the First and Second Observing Runs, *Phys. Rev. X* **9**, 031040 (2019), [arXiv:1811.12907 \[astro-ph.HE\]](#).
 - [3] S. Bird, I. Cholis, J. B. Muñoz, Y. Ali-Haïmoud, M. Kamionkowski, E. D. Kovetz, A. Raccanelli, and A. G. Riess, Did LIGO detect dark matter?, *Phys. Rev. Lett.* **116**, 201301 (2016), [arXiv:1603.00464 \[astro-ph.CO\]](#).
 - [4] M. Sasaki, T. Suyama, T. Tanaka, and S. Yokoyama, Primordial Black Hole Scenario for the Gravitational-Wave Event GW150914, *Phys. Rev. Lett.* **117**, 061101 (2016), [Erratum: *Phys.Rev.Lett.* 121, 059901 (2018)], [arXiv:1603.08338 \[astro-ph.CO\]](#).
 - [5] V. C. Rubin, N. Thonnard, and W. K. Ford, Jr., Rotational properties of 21 SC galaxies with a large range of luminosities and radii, from NGC 4605 / $R = 4$ kpc/ to UGC 2885 / $R = 122$ kpc/, *Astrophys. J.* **238**, 471 (1980).
 - [6] M. Persic, P. Salucci, and F. Stel, The Universal rotation curve of spiral galaxies: 1. The Dark matter connection, *Mon. Not. Roy. Astron. Soc.* **281**, 27 (1996), [arXiv:astro-ph/9506004](#).
 - [7] G. Bertone and D. Hooper, History of dark matter, *Rev. Mod. Phys.* **90**, 045002 (2018), [arXiv:1605.04909 \[astro-ph.CO\]](#).
 - [8] P. H. Frampton, M. Kawasaki, F. Takahashi, and T. T. Yanagida, Primordial Black Holes as All Dark Matter, *JCAP* **04**, 023 (2010), [arXiv:1001.2308 \[hep-ph\]](#).
 - [9] S. Clesse and J. García-Bellido, Massive Primordial Black Holes from Hybrid Inflation as Dark Matter and the seeds of Galaxies, *Phys. Rev. D* **92**, 023524 (2015), [arXiv:1501.07565 \[astro-ph.CO\]](#).
 - [10] K. Inomata, M. Kawasaki, K. Mukaida, Y. Tada, and T. T. Yanagida, Inflationary Primordial Black Holes as All Dark Matter, *Phys. Rev. D* **96**, 043504 (2017), [arXiv:1701.02544 \[astro-ph.CO\]](#).
 - [11] J. García-Bellido, Massive Primordial Black Holes as Dark Matter and their detection with Gravitational Waves, *J. Phys. Conf. Ser.* **840**, 012032 (2017), [arXiv:1702.08275 \[astro-ph.CO\]](#).
 - [12] E. D. Kovetz, Probing Primordial-Black-Hole Dark Matter with Gravitational Waves, *Phys. Rev. Lett.* **119**, 131301 (2017), [arXiv:1705.09182 \[astro-ph.CO\]](#).
 - [13] B. Carr, F. Kuhnel, and M. Sandstad, Primordial Black Holes as Dark Matter, *Phys. Rev. D* **94**, 083504 (2016), [arXiv:1607.06077 \[astro-ph.CO\]](#).
 - [14] B. Carr, K. Kohri, Y. Sendouda, and J. Yokoyama, Constraints on primordial black holes, *Rept. Prog. Phys.* **84**, 116902 (2021), [arXiv:2002.12778 \[astro-ph.CO\]](#).
 - [15] B. Carr and F. Kuhnel, Primordial Black Holes as Dark Matter: Recent Developments, *Ann. Rev. Nucl. Part. Sci.* **70**, 355 (2020), [arXiv:2006.02838 \[astro-ph.CO\]](#).
 - [16] Y. Ali-Haïmoud and M. Kamionkowski, Cosmic microwave background limits on accreting primordial black holes, *Phys. Rev. D* **95**, 043534 (2017), [arXiv:1612.05644 \[astro-ph.CO\]](#).
 - [17] V. Poulin, P. D. Serpico, F. Calore, S. Clesse, and K. Kohri, CMB bounds on disk-accreting massive primordial black holes, *Phys. Rev. D* **96**, 083524 (2017), [arXiv:1707.04206 \[astro-ph.CO\]](#).
 - [18] B. J. Carr, K. Kohri, Y. Sendouda, and J. Yokoyama, New cosmological constraints on primordial black holes, *Phys. Rev. D* **81**, 104019 (2010), [arXiv:0912.5297 \[astro-ph.CO\]](#).
 - [19] P. W. Graham, S. Rajendran, and J. Varela, Dark Matter Triggers of Supernovae, *Phys. Rev. D* **92**, 063007 (2015), [arXiv:1505.04444 \[hep-ph\]](#).
 - [20] H. Niikura et al., Microlensing constraints on primordial black holes with Subaru/HSC Andromeda observations, *Nature Astron.* **3**, 524 (2019), [arXiv:1701.02151 \[astro-ph.CO\]](#).
 - [21] K. Griest, A. M. Cieplak, and M. J. Lehner, New Limits on Primordial Black Hole Dark Matter from an Analysis of Kepler Source Microlensing Data, *Phys. Rev. Lett.* **111**, 181302 (2013).
 - [22] P. Tisserand et al. (EROS-2), Limits on the Macho Content of the Galactic Halo from the EROS-2 Survey of the Magellanic Clouds, *Astron. Astrophys.* **469**, 387 (2007), [arXiv:astro-ph/0607207](#).
 - [23] V. Vaskonen and H. Veermäe, Lower bound on the primordial black hole merger rate, *Phys. Rev. D* **101**, 043015

- (2020).
- [24] A. M. Green and B. J. Kavanagh, Primordial Black Holes as a dark matter candidate, *J. Phys. G* **48**, 043001 (2021), [arXiv:2007.10722 \[astro-ph.CO\]](#).
 - [25] H. Niikura, M. Takada, S. Yokoyama, T. Sumi, and S. Masaki, Constraints on Earth-mass primordial black holes from OGLE 5-year microlensing events, *Phys. Rev. D* **99**, 083503 (2019).
 - [26] S. Hawking, Gravitationally collapsed objects of very low mass, *Mon. Not. Roy. Astron. Soc.* **152**, 75 (1971).
 - [27] J. Garcia-Bellido and E. Ruiz Morales, Primordial black holes from single field models of inflation, *Phys. Dark Univ.* **18**, 47 (2017), [arXiv:1702.03901 \[astro-ph.CO\]](#).
 - [28] H. Di and Y. Gong, Primordial black holes and second order gravitational waves from ultra-slow-roll inflation, *JCAP* **07**, 007 (2018), [arXiv:1707.09578 \[astro-ph.CO\]](#).
 - [29] M. Sasaki, T. Suyama, T. Tanaka, and S. Yokoyama, Primordial black holes—perspectives in gravitational wave astronomy, *Class. Quant. Grav.* **35**, 063001 (2018), [arXiv:1801.05235 \[astro-ph.CO\]](#).
 - [30] J. Garriga and A. Vilenkin, Black holes from nucleating strings, *Phys. Rev. D* **47**, 3265 (1993), [arXiv:hep-ph/9208212](#).
 - [31] A. Polnarev and R. Zembowicz, Formation of Primordial Black Holes by Cosmic Strings, *Phys. Rev. D* **43**, 1106 (1991).
 - [32] H. Deng, J. Garriga, and A. Vilenkin, Primordial black hole and wormhole formation by domain walls, *JCAP* **04**, 050 (2017), [arXiv:1612.03753 \[gr-qc\]](#).
 - [33] Y. N. Eroshenko, Spin of primordial black holes in the model with collapsing domain walls, *JCAP* **12**, 041 (2021), [arXiv:2111.03403 \[astro-ph.CO\]](#).
 - [34] M. Lewicki, P. Toczek, and V. Vaskonen, Primordial black holes from strong first-order phase transitions, *JHEP* **09**, 092 (2023), [arXiv:2305.04924 \[astro-ph.CO\]](#).
 - [35] J. Liu, L. Bian, R.-G. Cai, Z.-K. Guo, and S.-J. Wang, Primordial black hole production during first-order phase transitions, *Phys. Rev. D* **105**, L021303 (2022), [arXiv:2106.05637 \[astro-ph.CO\]](#).
 - [36] R. Saito and J. Yokoyama, Gravitational wave background as a probe of the primordial black hole abundance, *Phys. Rev. Lett.* **102**, 161101 (2009), [Erratum: *Phys. Rev. Lett.* **107**, 069901 (2011)], [arXiv:0812.4339 \[astro-ph\]](#).
 - [37] R. Saito and J. Yokoyama, Gravitational-Wave Constraints on the Abundance of Primordial Black Holes, *Prog. Theor. Phys.* **123**, 867 (2010), [Erratum: *Prog. Theor. Phys.* **126**, 351–352 (2011)], [arXiv:0912.5317 \[astro-ph.CO\]](#).
 - [38] N. Orlofsky, A. Pierce, and J. D. Wells, Inflationary theory and pulsar timing investigations of primordial black holes and gravitational waves, *Phys. Rev. D* **95**, 063518 (2017), [arXiv:1612.05279 \[astro-ph.CO\]](#).
 - [39] S. Wang, Y.-F. Wang, Q.-G. Huang, and T. G. F. Li, Constraints on the Primordial Black Hole Abundance from the First Advanced LIGO Observation Run Using the Stochastic Gravitational-Wave Background, *Phys. Rev. Lett.* **120**, 191102 (2018), [arXiv:1610.08725 \[astro-ph.CO\]](#).
 - [40] R.-g. Cai, S. Pi, and M. Sasaki, Gravitational Waves Induced by non-Gaussian Scalar Perturbations, *Phys. Rev. Lett.* **122**, 201101 (2019), [arXiv:1810.11000 \[astro-ph.CO\]](#).
 - [41] Z. Yi, Primordial black holes and scalar-induced gravitational waves from the generalized Brans-Dicke theory, *JCAP* **03**, 048 (2023), [arXiv:2206.01039 \[gr-qc\]](#).
 - [42] P. Amaro-Seoane et al. (LISA), Laser Interferometer Space Antenna, (2017), [arXiv:1702.00786 \[astro-ph.IM\]](#).
 - [43] W.-R. Hu and Y.-L. Wu, The Taiji Program in Space for gravitational wave physics and the nature of gravity, *Natl. Sci. Rev.* **4**, 685 (2017).
 - [44] J. Luo et al. (TianQin), TianQin: a space-borne gravitational wave detector, *Class. Quant. Grav.* **33**, 035010 (2016), [arXiv:1512.02076 \[astro-ph.IM\]](#).
 - [45] S. Kawamura et al., The Japanese space gravitational wave antenna DECIGO, *Class. Quant. Grav.* **23**, S125 (2006).
 - [46] W.-T. Xu, J. Liu, T.-J. Gao, and Z.-K. Guo, Gravitational waves from double-inflection-point inflation, *Phys. Rev. D* **101**, 023505 (2020), [arXiv:1907.05213 \[astro-ph.CO\]](#).
 - [47] L. Anguelova, On Primordial Black Holes from Rapid Turns in Two-field Models, *JCAP* **06**, 004 (2021), [arXiv:2012.03705 \[hep-th\]](#).
 - [48] J.-X. Zhao, X.-H. Liu, and N. Li, Primordial black holes and scalar-induced gravitational waves from the perturbations on the inflaton potential in peak theory, *Phys. Rev. D* **107**, 043515 (2023), [arXiv:2302.06886 \[astro-ph.CO\]](#).
 - [49] C. Chen, A. Ghoshal, Z. Lalak, Y. Luo, and A. Naskar, Growth of curvature perturbations for PBH formation & detectable GWs in non-minimal curvaton scenario revisited, *JCAP* **08**, 041 (2023), [arXiv:2305.12325 \[astro-ph.CO\]](#).
 - [50] Z. Yi, Q. Gao, Y. Gong, and Z.-h. Zhu, Primordial black holes and scalar-induced secondary gravitational waves from inflationary models with a noncanonical kinetic term, *Phys. Rev. D* **103**, 063534 (2021), [arXiv:2011.10606 \[astro-ph.CO\]](#).
 - [51] S. S. Mishra and V. Sahni, Primordial Black Holes from a tiny bump/dip in the Inflaton potential, *JCAP* **04**, 007 (2020), [arXiv:1911.00057 \[gr-qc\]](#).
 - [52] C. Fu and C. Chen, Sudden braking and turning with a two-field potential bump: primordial black hole formation, *JCAP* **05**, 005 (2023), [arXiv:2211.11387 \[astro-ph.CO\]](#).
 - [53] Q. Wang, Y.-C. Liu, B.-Y. Su, and N. Li, Primordial black holes from the perturbations in the inflaton potential in peak theory, *Phys. Rev. D* **104**, 083546 (2021), [arXiv:2111.10028 \[astro-ph.CO\]](#).
 - [54] A. A. Starobinsky, A New Type of Isotropic Cosmological Models Without Singularity, *Phys. Lett. B* **91**, 99 (1980).
 - [55] S. S. Mishra, V. Sahni, and A. V. Toporensky, Initial conditions for Inflation in an FRW Universe, *Phys. Rev. D* **98**, 083538 (2018), [arXiv:1801.04948 \[gr-qc\]](#).
 - [56] V. F. Mukhanov, Gravitational Instability of the Universe Filled with a Scalar Field, *JETP Lett.* **41**, 493 (1985).
 - [57] M. Sasaki, Large Scale Quantum Fluctuations in the Inflationary Universe, *Prog. Theor. Phys.* **76**, 1036 (1986).
 - [58] Y. Akrami et al. (Planck), Planck 2018 results. X. Constraints on inflation, *Astron. Astrophys.* **641**, A10 (2020), [arXiv:1807.06211 \[astro-ph.CO\]](#).
 - [59] P. A. R. Ade et al. (BICEP2, Keck Array), BICEP2 / Keck Array x: Constraints on Primordial Gravitational Waves using Planck, WMAP, and New BICEP2/Keck Observations through the 2015 Season, *Phys. Rev. Lett.* **121**, 221301 (2018), [arXiv:1810.05216 \[astro-ph.CO\]](#).
 - [60] K. Inomata and T. Nakama, Gravitational waves induced by scalar perturbations as probes of the small-scale primordial spectrum, *Phys. Rev. D* **99**, 043511 (2019), [arXiv:1812.00674 \[astro-ph.CO\]](#).

- [61] K. Inomata, M. Kawasaki, and Y. Tada, Revisiting constraints on small scale perturbations from big-bang nucleosynthesis, *Phys. Rev. D* **94**, 043527 (2016), [arXiv:1605.04646 \[astro-ph.CO\]](#).
- [62] D. J. Fixsen, E. S. Cheng, J. M. Gales, J. C. Mather, R. A. Shafer, and E. L. Wright, The Cosmic Microwave Background spectrum from the full COBE FIRAS data set, *Astrophys. J.* **473**, 576 (1996), [arXiv:astro-ph/9605054](#).
- [63] W. H. Press and P. Schechter, Formation of galaxies and clusters of galaxies by selfsimilar gravitational condensation, *Astrophys. J.* **187**, 425 (1974).
- [64] T. Harada, C.-M. Yoo, and K. Kohri, Threshold of primordial black hole formation, *Phys. Rev. D* **88**, 084051 (2013), [Erratum: *Phys.Rev.D* **89**, 029903 (2014)], [arXiv:1309.4201 \[astro-ph.CO\]](#).
- [65] B. J. Carr, The Primordial black hole mass spectrum, *Astrophys. J.* **201**, 1 (1975).
- [66] N. Aghanim et al. (Planck), Planck 2018 results. VI. Cosmological parameters, *Astron. Astrophys.* **641**, A6 (2020), [Erratum: *Astron.Astrophys.* **652**, C4 (2021)], [arXiv:1807.06209 \[astro-ph.CO\]](#).
- [67] J. Scholtz and J. Unwin, What if Planet 9 is a Primordial Black Hole?, *Phys. Rev. Lett.* **125**, 051103 (2020), [arXiv:1909.11090 \[hep-ph\]](#).
- [68] K. Kohri and T. Terada, Semianalytic calculation of gravitational wave spectrum nonlinearly induced from primordial curvature perturbations, *Phys. Rev. D* **97**, 123532 (2018), [arXiv:1804.08577 \[gr-qc\]](#).
- [69] K. N. Ananda, C. Clarkson, and D. Wands, The Cosmological gravitational wave background from primordial density perturbations, *Phys. Rev. D* **75**, 123518 (2007), [arXiv:gr-qc/0612013](#).
- [70] D. Baumann, P. J. Steinhardt, K. Takahashi, and K. Ichiki, Gravitational Wave Spectrum Induced by Primordial Scalar Perturbations, *Phys. Rev. D* **76**, 084019 (2007), [arXiv:hep-th/0703290](#).
- [71] A. Ali, Y.-P. Hu, M. Sabir, and T. Sui, On the gauge dependence of scalar induced secondary gravitational waves during radiation and matter domination eras, *Sci. China Phys. Mech. Astron.* **66**, 290411 (2023), [arXiv:2308.04713 \[gr-qc\]](#).
- [72] Y. Lu, A. Ali, Y. Gong, J. Lin, and F. Zhang, Gauge transformation of scalar induced gravitational waves, *Phys. Rev. D* **102**, 083503 (2020), [arXiv:2006.03450 \[gr-qc\]](#).
- [73] C. Fu, P. Wu, and H. Yu, Scalar induced gravitational waves in inflation with gravitationally enhanced friction, *Phys. Rev. D* **101**, 023529 (2020), [arXiv:1912.05927 \[astro-ph.CO\]](#).
- [74] F. Zhang, Primordial black holes and scalar induced gravitational waves from the E model with a Gauss-Bonnet term, *Phys. Rev. D* **105**, 063539 (2022), [arXiv:2112.10516 \[gr-qc\]](#).
- [75] G. Hobbs et al., The international pulsar timing array project: using pulsars as a gravitational wave detector, *Class. Quant. Grav.* **27**, 084013 (2010), [arXiv:0911.5206 \[astro-ph.SR\]](#).
- [76] M. A. McLaughlin, The North American Nanohertz Observatory for Gravitational Waves, *Class. Quant. Grav.* **30**, 224008 (2013), [arXiv:1310.0758 \[astro-ph.IM\]](#).
- [77] G. Hobbs, The Parkes Pulsar Timing Array, *Class. Quant. Grav.* **30**, 224007 (2013), [arXiv:1307.2629 \[astro-ph.IM\]](#).
- [78] R. D. Ferdman et al., The European Pulsar Timing Array: current efforts and a LEAP toward the future, *Class. Quant. Grav.* **27**, 084014 (2010), [arXiv:1003.3405 \[astro-ph.HE\]](#).
- [79] L. Lentati et al. (EPTA), European Pulsar Timing Array Limits On An Isotropic Stochastic Gravitational-Wave Background, *Mon. Not. Roy. Astron. Soc.* **453**, 2576 (2015), [arXiv:1504.03692 \[astro-ph.CO\]](#).
- [80] R. M. Shannon et al., Gravitational waves from binary supermassive black holes missing in pulsar observations, *Science* **349**, 1522 (2015), [arXiv:1509.07320 \[astro-ph.CO\]](#).
- [81] C. J. Moore, R. H. Cole, and C. P. L. Berry, Gravitational-wave sensitivity curves, *Class. Quant. Grav.* **32**, 015014 (2015), [arXiv:1408.0740 \[gr-qc\]](#).
- [82] Z. Arzoumanian et al. (NANOGrav), The NANOGrav 12.5 yr Data Set: Search for an Isotropic Stochastic Gravitational-wave Background, *Astrophys. J. Lett.* **905**, L34 (2020), [arXiv:2009.04496 \[astro-ph.HE\]](#).
- [83] V. De Luca, G. Franciolini, A. Kehagias, M. Peloso, A. Riotto, and C. Ünal, The Ineludible non-Gaussianity of the Primordial Black Hole Abundance, *JCAP* **07**, 048 (2019), [arXiv:1904.00970 \[astro-ph.CO\]](#).
- [84] T. Matsubara and M. Sasaki, Non-Gaussianity effects on the primordial black hole abundance for sharply-peaked primordial spectrum, *JCAP* **10**, 094 (2022), [arXiv:2208.02941 \[astro-ph.CO\]](#).
- [85] Y.-F. Cai, X. Chen, M. H. Namjoo, M. Sasaki, D.-G. Wang, and Z. Wang, Revisiting non-Gaussianity from non-attractor inflation models, *JCAP* **05**, 012 (2018), [arXiv:1712.09998 \[astro-ph.CO\]](#).
- [86] G. Franciolini, A. Kehagias, S. Matarrese, and A. Riotto, Primordial Black Holes from Inflation and non-Gaussianity, *JCAP* **03**, 016 (2018), [arXiv:1801.09415 \[astro-ph.CO\]](#).
- [87] J. M. Bardeen, J. R. Bond, N. Kaiser, and A. S. Szalay, The Statistics of Peaks of Gaussian Random Fields, *Astrophys. J.* **304**, 15 (1986).
- [88] A. M. Green, A. R. Liddle, K. A. Malik, and M. Sasaki, A New calculation of the mass fraction of primordial black holes, *Phys. Rev. D* **70**, 041502 (2004), [arXiv:astro-ph/0403181](#).